

CamoFormer: Masked Separable Attention for Camouflaged Object Detection

Bowen Yin¹ Xuying Zhang¹ Qibin Hou^{1*} Bo-Yuan Sun¹ Deng-Ping Fan² Luc Van Gool²

¹ TMCC, School of Computer Science, Nankai University
² ETH Zurich

<https://github.com/HVision-NKU/CamoFormer>

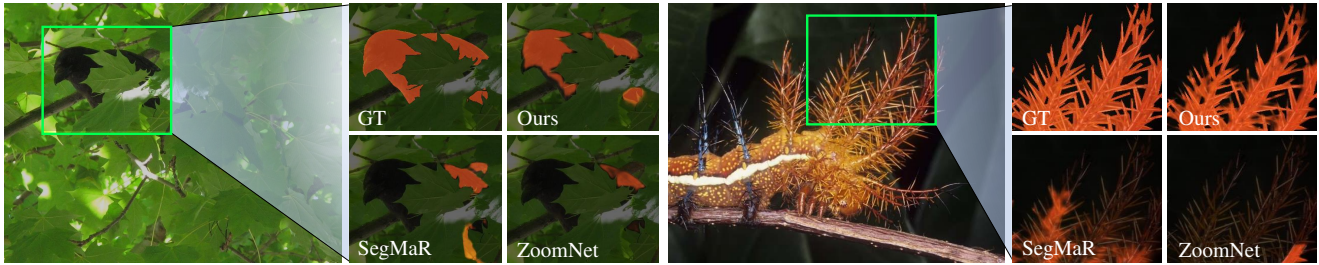


Figure 1. Visual comparison between our CamoFormer and recent state-of-the-art methods (*e.g.*, SegMaR [22] and ZoomNet [41]) for camouflaged object detection. The segmentation details of different methods in the green rectangle regions are displayed with focus views. We can easily observe that our CamoFormer can generate much better results than other methods. Best viewed in color.

Abstract

How to identify and segment camouflaged objects from the background is challenging. Inspired by the multi-head self-attention in Transformers, we present a simple masked separable attention (MSA) for camouflaged object detection. We first separate the multi-head self-attention into three parts, which are responsible for distinguishing the camouflaged objects from the background using different mask strategies. Furthermore, we propose to capture high-resolution semantic representations progressively based on a simple top-down decoder with the proposed MSA to attain precise segmentation results. These structures plus a backbone encoder form a new model, dubbed **CamoFormer**. Extensive experiments show that CamoFormer surpasses all existing state-of-the-art methods on three widely-used camouflaged object detection benchmarks. There are on average $\sim 5\%$ relative improvements over previous methods in terms of *S*-measure and weighted *F*-measure.

1. Introduction

Camouflaged object detection (COD) is a new challenging task [10] that has been popular in recent years [10–12, 20, 40]. Biological studies have shown that the human visual perceptual system can be easily deceived [48] by var-

ious camouflage strategies in that camouflaged objects are highly similar to their surroundings or extremely small in size. The high similarity between the camouflaged objects and their surroundings makes the COD [11] more challenging than traditional object detection [31, 39], attracting more and more research attention, such as medical image segmentation [12] and search engine [10].

There are an increasing number of works using sophisticated deep learning techniques [40, 41, 70] to solve this task, especially after a large-scale dataset was proposed [10]. However, even the state-of-the-art (SOTA) methods are still struggled to segment camouflaged targets with fine shapes for some complex scenes, as shown in Fig. 1. We argue that an important reason is that these models cope with the foreground and background cues indiscriminately, making them difficult to identify the camouflaged objects from similar surroundings. The key to solving this issue is to encode the foreground and background cues separately.

Taking the aforementioned analysis into account, in this paper, we present *Masked Separable Attention (MSA)* to explicitly process the camouflaged objects and background based on the Multi-Dconv Head Transposed Attention [63]. Instead of performing the same operations in each head, our MSA separates the attention heads into three groups, each of which is responsible for specific functionality. In particular, inspired by masked attention [3], we propose to use two groups of heads to process the foreground and back-

*Qibin Hou is the corresponding author.

ground regions independently. Our goal is to use the attention scores built within the predicted foreground generated by a prediction head to discover camouflaged objects from the full-value representations and vice versa for the background. Besides, we keep a group of normal attention heads for building global interactions, which is essential for generating high-quality segmentation maps.

Given the proposed MSA, we apply it to an encoder-decoder architecture [29,30] to progressively refine the segmentation map as illustrated in Fig. 2. At each feature level of the decoder, a segmentation map is predicted and sent to an MSA block to improve the prediction quality. This progressive refinement process enables us to attain high-quality camouflaged object predictions as the feature resolution increases. As shown in Fig. 1, our CamoFormer can more accurately identify the camouflaged objects and generate segmentation maps with finer borders than other cutting-edge methods.

To validate the effectiveness of our CamoFormer, we conduct extensive experiments on three popular COD benchmarks (NC4K [36], COD10K [11], and CAMO [27]). On all these benchmarks, CamoFormer achieves new state-of-the-art (SOTA) records compared to the recent methods. In particular, our method achieves 0.786 weighted F-measure and 0.023 MAE, while the corresponding results for the second-best model FNet [70] are 0.731 and 0.030 on the COD10K-test dataset. Furthermore, the visualization results also show the superiority of our CamoFormer over existing COD methods. To sum up, our main contributions can be summarized as follows:

- We present masked separable attention (MSA). It divides the attention heads into three groups and discovers the foreground and background regions by separately computing their attention scores via a predicted map for accurate segmentation;
- We adopt a progressive refinement manner to make better use of our MSA, which can gradually improve the segmentation results predicted at each feature level;
- Our CamoFormer improves all the recent SOTA methods by a large margin on all these three COD benchmarks. Visualization experiments further illustrate the superiority of CamoFormer on the completeness of the segments.

2. Related Work

2.1. Camouflaged Object Detection

Traditional COD methods [1, 13–15, 25, 68] extract various hand-crafted features between the camouflaged objects and backgrounds to segment the camouflaged targets. These

methods can deal with simple scenes, but show drastic performance degradation in complex conditions.

Recently, the mainstream in COD is CNN-based approaches [11, 21, 22, 40, 41, 66, 70], which can be categorized into three strategies: i) multi-scale feature aggregation: CubeNet [72] accompanies attention fusion and X-shaped connection to integrate features from multiple layers sufficiently. ZoomNet [41] processes the input images at three scales and unifies the scale-specific appearance features at different scales. ii) Multi-stage strategy: Due to the concealment of camouflaged objects, SINet [11] proposes first to locate and then distinguish them for better performance. PreyNet [66] mimics the process of predation and splits the detection process of camouflaged targets into initial detection and predator learning. SINetV2 [10] adopts surrounding connection decoder and group-reversal attention to improve the performance. SegMaR [22], a multi-stage training and inference framework, locates the target and magnifies the object regions to detect camouflaged objects progressively. iii) Joint training strategy: UJSC [28] leverages the contradictory information to enhance the detection ability for both salient object detection and camouflaged object detection.

2.2. Transformers in Computer Vision

Transformer architectures are initially designed for natural language processing [6, 52] and then get popular in computer vision [4, 16, 47, 56, 59, 61]. Compared with conventional convolutional neural networks [17, 19, 44, 45, 50], Transformers can efficiently encode global contextual information and hence have been widely used in a variety of visual tasks, including image classification [7, 51, 54, 62], semantic segmentation [24, 57, 69], object detection [2], and salient object detection [32, 71].

Transformer-based models are also becoming a new trend in COD. UGTR [60] explicitly utilizes the probabilistic representational model to learn the uncertainties of the camouflaged object under the Transformer framework. DTINet [35] designs a dual-task interactive Transformer to segment both the camouflaged objects and their detailed borders. TPRNet [67] proposes a transformer-induced progressive refinement network that utilizes the semantic information from high-level features to guide the detection of camouflaged targets.

Our CamoFormer is also built upon the popular Transformer framework. Not focusing on a novel architecture design, we aim to investigate more efficient ways to utilize self-attention for COD and receive better performance than other methods. We assign different functionalities to different attention heads to process the foreground and background regions separately, which makes our work quite different from other Transformer-based COD methods.

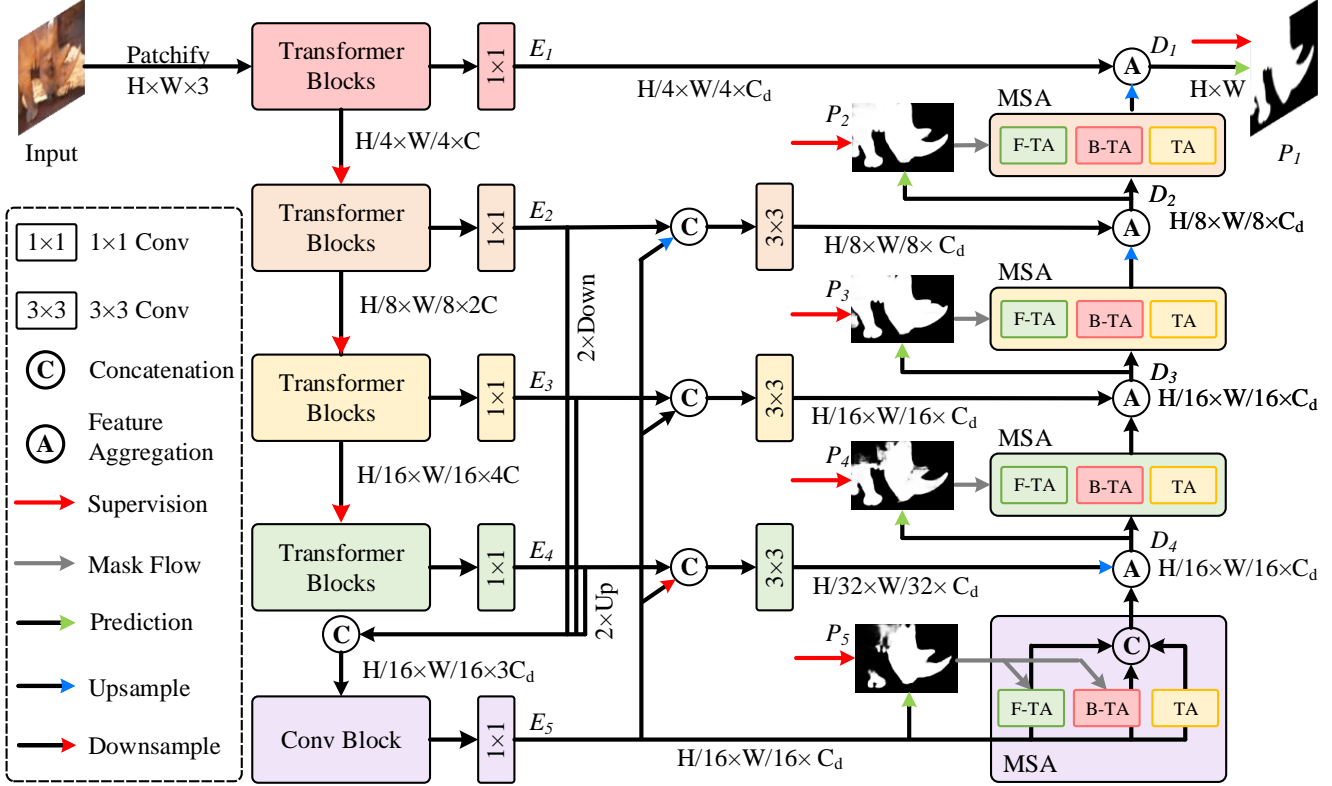


Figure 2. Overall architecture of our CamoFormer model. First, a pretrained Transformer-based backbone is utilized to extract multi-scale features of the input image. Then, the features from the last three stages are aggregated to generate the coarse prediction. Next, the progressive refinement decoder equipped with masked separable attention (MSA) is applied to gradually polish the prediction results. All the predictions generated by our CamoFormer are supervised by the ground truth (GT).

3. Proposed CamoFormer

Similar to most previous works [11, 12, 23, 41, 70], we adopt an encoder-decoder architecture to build our CamoFormer. Our CamoFormer is an end-to-end trainable framework, which is shown in Fig. 2.

3.1. Overall Architecture

Encoder. By default, we adopt the PVTv2 [55] as our encoder, as vision transformers have shown great performance in binary segmentation tasks [32, 65]. Given an input image $I \in \mathbb{R}^{H \times W \times 3}$, we feed it into the encoder to generate multi-scale feature maps from the four stages, which are denoted as $\{E_i\}_{i=1}^4$. Consequently, E_1 is with spatial size $\frac{H}{4} \times \frac{W}{4}$ and E_4 is with spatial size $\frac{H}{32} \times \frac{W}{32}$. Then, we aggregate the features from the last three stages of the encoder and send them to a convolutional block, yielding representations E_5 with higher-level semantics.

Decoder. The decoder is built upon the encoder. The multi-level semantic features $\{E_i\}_{i=1}^5$ from the encoder are fed into the decoder. To achieve a better trade-off between ef-

iciency and performance, we first connect a 1×1 convolution with $C_d = 128$ channels to the feature maps at each level. As shown in Fig. 2, we adopt a progressive way to refine the features from the top of the encoder. At each feature level, masked separable attention (MSA) is used for a better distinction of the camouflaged objects and the background. In the initial level of progressive fusion, the aggregated feature D_4 can be written as:

$$D_4 = \text{MSA}(E_5) \cdot \mathcal{F}_{\text{up}}(E_4) + \mathcal{F}_{\text{up}}(E_4), \quad (1)$$

where $\mathcal{F}_{\text{up}}(\cdot)$ is a bilinear upsampling operation for shape matching. And the aggregated features $\{D_i\}_{i=1}^3$ in the following levels can be defined as:

$$D_i = \mathcal{F}_{\text{up}}(\text{MSA}(D_{i+1})) \cdot E_i + E_i. \quad (2)$$

Unlike previous works [11, 22, 41] that mainly use the addition operation or the concatenation operation to fuse the features from different feature levels, we first compute the element-wise product between them and then use the summation operation. We empirically found that such a simple modification brings about 0.2%+ relative improvement in

terms of S-measure and weighted F-measure averagely on NC4K [36], COD10K-test [10], and CAMO-test [27].

Loss Function. Following [18,58], we add side supervision at each feature level. We denote the predictions generated by the decoder of CamoFormer as $\{P_i\}_{i=1}^5$. Except for the final prediction map P_1 , all the other prediction maps P_i are used in the MSAs for the progressive refinement as described above. During training, each P_i is rescaled to the same size as the input image and all of them are supervised by the BCE loss [5] and IoU loss [38]. Following [10], the overall loss is a summation of multi-stage loss. The total loss of our CamoFormer can be formulated as follows:

$$\mathcal{L}(P, G) = \sum_{i=1}^5 \mathcal{L}_{bce}(P_i, G) + \mathcal{L}_{iou}(P_i, G), \quad (3)$$

where G is the ground truth annotation.

3.2. Masked Separable Attention

Camouflaged objects are diverse in scale and highly similar to the background, which makes them difficult to segment completely. How to accurately identify camouflaged objects from the background is crucial. We solve this by presenting masked separable attention (MSA), where different attention heads take charge of different functionalities. Our intention is to use part of the attention heads to separately calculate the attention scores in the predicted foreground and background regions and use them to identify the camouflaged objects better.

Our MSA is based on a modified version of self-attention to save computations, namely Multi-Dconv Head Transposed Attention [63], which we denote as TA for short. Given an input $\mathbf{X} \in \mathbb{R}^{H \times W \times C}$ where H and W are respectively the height and width while C is the channel number, the TA is formulated as:

$$\text{TA}(\mathbf{Q}, \mathbf{K}, \mathbf{V}) = \mathbf{V} \cdot \text{Softmax}\left(\frac{\mathbf{Q}^\top \mathbf{K}}{\alpha}\right), \quad (4)$$

where $\mathbf{Q}, \mathbf{K}, \mathbf{V}$ are the query, key, value matrices that can be generated by using three separate 1×1 convolutions followed by a 3×3 depthwise convolution, and α is a learnable scaling parameter. In practical use, Eqn. 4 can also be extended to a multi-head version, as done in the original self-attention [52], to augment the feature representations.

Masked Separable Attention. The attention heads in the above TA are equally utilized for encoding spatial information. Differently, in our MSA, we propose to introduce a prediction mask which can be generated at each feature level into TA as a foreground-background contrast prior for better recognizing the camouflaged objects. To achieve this, we divide all the attention heads into three groups:

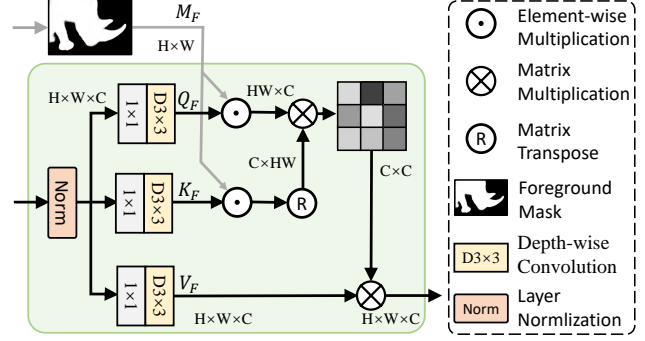


Figure 3. Diagrammatic details of the proposed F-TA in our MSA. Our B-TA shares a similar structure except for the mask.

foreground-head TA (F-TA), background-head TA (B-TA), and the normal TA. The structural details of our MSA are shown in Fig. 3.

To be specific, given a predicted foreground mask M_F , the formulation of F-TA can be written as:

$$\text{F-TA}(\mathbf{Q}_F, \mathbf{K}_F, \mathbf{V}_F) = \mathbf{V}_F \cdot \text{Softmax}\left(\frac{\mathbf{Q}_F^\top \mathbf{K}_F}{\alpha_F}\right), \quad (5)$$

where $\mathbf{Q}_F, \mathbf{K}_F$ are the masked query and key matrices that can be produced by multiplying them with M_F and \mathbf{V}_F is the value matrix without masking. In this way, the features can be refined by building pairwise relationships within the foreground regions, avoiding the influence of the background which may contain contaminative information. Similarly, given the background mask via the broadcast subtraction $M_B = 1 - M_F$, we can also conduct this process for the background. Thus, the formulation of B-TA can be written as:

$$\text{B-TA}(\mathbf{Q}_B, \mathbf{K}_B, \mathbf{V}_B) = \mathbf{V}_B \cdot \text{Softmax}\left(\frac{\mathbf{Q}_B^\top \mathbf{K}_B}{\alpha_B}\right). \quad (6)$$

Other than the F-TA heads and B-TA heads, the third group of the heads is kept unchanged as in Eqn. 4, which is used to build relationships between the foreground and background. The outputs of all the heads are then concatenated and sent into a 3×3 convolution for feature aggregation and map the number of channels to C_d :

$$\mathbf{Z} = \text{Conv}_{3 \times 3}([\text{F-TA}, \text{B-TA}, \text{TA}]), \quad (7)$$

where $[\dots]$ is the concatenation operation.

Mask Generation. At each feature level, a mask should be generated by a 3×3 convolution following a Sigmoid function and then used in our MSA. As supervision is added to each feature level, we directly use the predictions $\{P_i\}_{i=2}^5$ as masks and sent each of them to the corresponding MSA. Note that we do not binarize the prediction maps but keep them as continuous maps ranging from 0 to 1, which we found works better during our experiments.

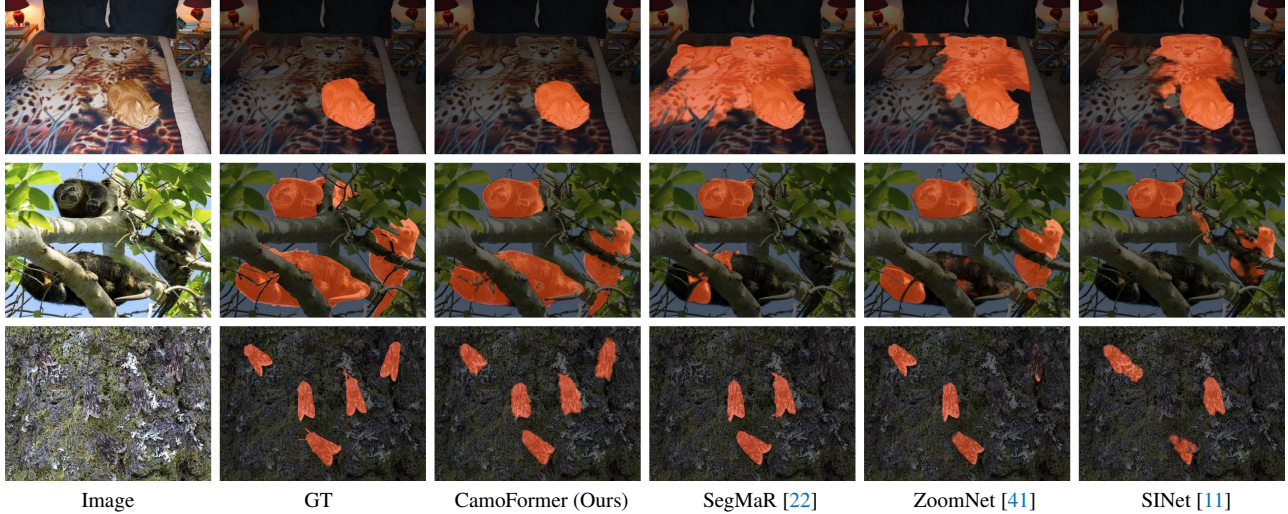


Figure 4. Visualization comparisons between our CamoFormer and other SOTA methods. Segmentation results are shown in orange.

4. Experimental Results

4.1. Experiment Setup

Implementation Details. We implement our CamoFormer using the Pytorch library [42]. A pretrained PVTv2 [55] on the ImageNet dataset [26] is employed as the encoder of our network. Unless otherwise specified, we adopt PVTv2 [55] as the backbone. Besides, we also report results with other backbones, *e.g.* Transformer-based Swin Transformer [33], CNN-based ResNet [17] and ConvNeXt [34]. SGD with momentum 0.9 and weight decay $2e-4$ is used as the optimizer. The learning rate is initially set to $5e-3$ and decays following the cosine learning rate strategy. During training, all the input images are resized to 384×384 . The entire model is trained end-to-end for 60 epochs costing around 7 hours with a batch size of 6 on an NVIDIA V100 GPU.

Datasets. We evaluate our methods on three popular COD benchmarks, including CAMO [27], COD10K [10], and NC4k [36]. CAMO comprises 2,500 images, half of which contain camouflaged objects and half do not. COD10k includes 5,066 camouflaged, 3,000 background, and 1,934 non-camouflaged images. NC4K is a large-scale COD dataset consisting of 4,121 images for testing. Following previous works [11, 22, 41], we use 1,000 images from the CAMO dataset and 3,040 images from COD10K for training and the others for testing.

Metrics. Following [22, 41, 70], we use four golden metrics for evaluation, including Structure-measure (S_m) [8], mean absolute error (M) [43], weighted F-measure (wF) [37], and adaptive E-measure (αE) [9]. M is the absolute difference between the prediction map and GT. S_m simultaneously evaluates region-aware and object-aware structural similarity between predictions and GT. wF is an exhaustive mea-

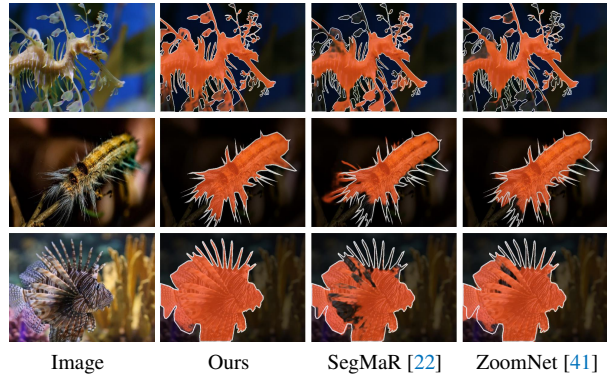


Figure 5. Comparisons of our CamoFormer and other SOTA methods on the borders of segmentation. The borders of GT are marked in white, and the ones of predictions are in orange.

sure of both recall and precision. αE evaluates element-wise similarity and the statistics at the image level. In addition, we draw the precision-recall (PR) curves and F_β -threshold (F_β) curves in the supplementary materials.

4.2. Qualitative Evaluation

Visualization of Predictions. Fig. 4 presents the visualization samples of our CamoFormer and three previous SOTA methods. In order to better show the performance of these models, several typical samples containing different complex scenarios in the COD field are selected. As shown in the top row, other methods are struggled to precisely perceive the camouflaged objects from their similar surroundings. Sometimes, it is also difficult for them to identify the camouflaged objects owing to the lack of global contrast information, as shown in the bottom two rows. In short, they misjudge some regions or miss parts of the

Method	NC4K (4,121)				COD10K-Test (2,026)				CAMO-Test (250)			
	$S_m \uparrow$	$\alpha E \uparrow$	$wF \uparrow$	$M \downarrow$	$S_m \uparrow$	$\alpha E \uparrow$	$wF \uparrow$	$M \downarrow$	$S_m \uparrow$	$\alpha E \uparrow$	$wF \uparrow$	$M \downarrow$
<i>CNN-Based Methods</i>												
PraNet ₂₀₂₀ [12]	0.822	0.871	0.724	0.059	0.789	0.839	0.629	0.045	0.769	0.833	0.663	0.094
SINet ₂₀₂₀ [11]	0.808	0.883	0.723	0.058	0.776	0.867	0.631	0.043	0.745	0.825	0.644	0.092
SLSR ₂₀₂₁ [36]	0.840	0.902	0.766	0.048	0.804	0.882	0.673	0.037	0.787	0.855	0.696	0.080
MGL-R ₂₀₂₁ [64]	0.833	0.893	0.739	0.053	0.814	0.865	0.666	0.035	0.782	0.847	0.695	0.085
PFNet ₂₀₂₁ [40]	0.829	0.892	0.745	0.053	0.800	0.868	0.660	0.040	0.782	0.852	0.695	0.085
UJSC ₂₀₂₁ [28]	0.842	0.907	0.771	0.047	0.809	0.891	0.684	0.035	0.800	0.853	0.728	0.073
C²FNet ₂₀₂₁ [49]	0.838	0.898	0.762	0.049	0.813	0.886	0.686	0.036	0.796	0.864	0.719	0.080
SINetV2 ₂₀₂₂ [10]	0.847	0.898	0.770	0.048	0.815	0.863	0.680	0.037	0.820	0.875	0.743	0.070
DGNet ₂₀₂₂ [20]	0.857	0.907	0.784	0.042	0.822	0.877	0.693	0.033	0.839	0.901	0.769	0.057
SegMaR ₂₀₂₂ [22]	0.841	0.905	0.781	0.046	0.833	0.895	0.724	0.033	0.815	0.872	0.742	0.071
ZoomNet ₂₀₂₂ [41]	0.853	0.907	0.784	0.043	0.838	0.893	0.729	0.029	0.820	0.883	0.752	0.066
FDNet ₂₀₂₂ [70]	0.834	0.895	0.750	0.052	0.837	0.897	0.731	0.030	0.844	0.903	0.778	0.062
CamoFormer-R (Ours)	0.857	0.915	0.793	0.041	0.838	0.898	0.730	0.029	0.817	0.884	0.756	0.066
CamoFormer-C (Ours)	0.884	0.936	0.833	0.033	0.860	0.923	0.767	0.024	0.860	0.920	0.811	0.051
<i>Transformer-Based Methods</i>												
COS-T ₂₀₂₁ [53]	0.825	0.881	0.730	0.055	0.790	0.901	0.693	0.035	0.813	0.896	0.776	0.060
VST ₂₀₂₁ [32]	0.830	0.887	0.740	0.053	0.810	0.866	0.680	0.035	0.805	0.863	0.780	0.069
UGTR ₂₀₂₁ [60]	0.839	0.886	0.746	0.052	0.817	0.850	0.666	0.036	0.784	0.859	0.794	0.086
ICON ₂₀₂₂ [71]	0.858	0.914	0.782	0.041	0.818	0.882	0.688	0.033	0.840	0.902	0.769	0.058
TPRNet ₂₀₂₂ [67]	0.854	0.903	0.790	0.047	0.829	0.892	0.725	0.034	0.814	0.870	0.781	0.076
DTINet ₂₀₂₂ [35]	0.863	0.915	0.792	0.041	0.824	0.893	0.695	0.034	0.857	0.912	0.796	0.050
CamoFormer-S (Ours)	0.888	0.941	0.840	0.031	0.862	0.932	0.772	0.024	0.876	0.935	0.832	0.043
CamoFormer-P (Ours)	0.892	0.941	0.847	0.030	0.869	0.931	0.786	0.023	0.872	0.931	0.831	0.046

Table 1. Comparison of our CamoFormer with the recent SOTA methods. ‘-R’: ResNet [17], ‘-C’: ConvNext [34], ‘-S’: Swin Transformer [33], ‘-P’: PVTv2 [55]. As can be seen, our CamoFormer-P performs much better than previous methods with either CNN- or Transformer-based models. ‘ \uparrow ’: the higher the better, ‘ \downarrow ’: the lower the better.

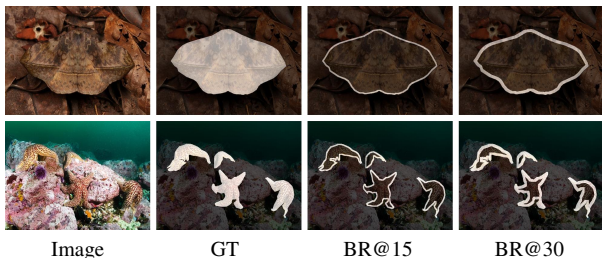


Figure 6. Illustration for the region of borders. ‘BR@15’ and ‘BR@30’ are border regions that are generated by dilating the borders of GT via 15×15 and 30×30 dilation kernels respectively.

targets when dealing with complex conditions due to the lack of a comprehensive understanding of the foreground and background. In contrast, by explicitly perceiving the foreground-background clues, our CamoFormer can generate high-quality segmentation maps of the camouflaged objects even under difficult conditions.

Object Border Quality Comparison. Camouflaged objects sometimes possess peculiar-looking shapes, as shown in Fig. 5. To demonstrate how well our CamoFormer performs when coping with these kinds of objects, we show some prediction results in Fig. 5 and depict the GT object

Method	BR@15		BR@30	
	BR- $wF \uparrow$	BR-M \downarrow	BR- $wF \uparrow$	BR-M \downarrow
SINet ₂₀₂₀ [11]	0.645	0.103	0.707	0.069
PFNet ₂₀₂₁ [40]	0.677	0.091	0.736	0.064
ZoomNet ₂₀₂₂ [41]	0.716	0.074	0.762	0.059
UGTR ₂₀₂₁ [60]	0.672	0.084	0.720	0.063
DTINet ₂₀₂₂ [35]	0.726	0.074	0.770	0.054
CamoFormer-P (Ours)	0.777	0.061	0.818	0.043

Table 2. Comparison of our CamoFormer-P with other methods in terms of BR- wF and BR-M on the NC4K dataset [36].

borders with white curves. The borders of our predictions are closer to those of the GT objects, while there are obvious deviations in the predictions by other methods. These visualizations indicate that our model can segment more precise camouflaged targets.

4.3. Quantitative Evaluation

We compare our CamoFormer with 12 CNN-based SOTA COD models, including ZoomNet [41], FDNet [70], SegMaR [22], DGNet [20], SINetV2 [10], C²FNet [49], UJSC [28], PFNet [40], MGL-R [64], SLSR [36], SINet [11], and PraNet [12] and 6 Transformer-based methods, including COS-T [53], TPRNet [67], VST [32],

Setting	NC4K (4,121)				COD10K-Test (2,026)				CAMO-Test (250)			
	$S_m \uparrow$	$\alpha E \uparrow$	$wF \uparrow$	$M \downarrow$	$S_m \uparrow$	$\alpha E \uparrow$	$wF \uparrow$	$M \downarrow$	$S_m \uparrow$	$\alpha E \uparrow$	$wF \uparrow$	$M \downarrow$
Baseline	0.859	0.916	0.801	0.043	0.830	0.904	0.719	0.032	0.838	0.891	0.780	0.058
Baseline+MSA	0.875	0.926	0.808	0.036	0.848	0.906	0.735	0.029	0.858	0.918	0.798	0.052
CamoFormer-P w/ TA only	0.880	0.925	0.825	0.034	0.850	0.908	0.749	0.026	0.862	0.918	0.812	0.055
CamoFormer-P	0.892	0.941	0.847	0.030	0.869	0.931	0.786	0.023	0.872	0.931	0.831	0.046

Table 3. Ablation study of our CamoFormer variants. ‘Baseline’: the transformer backbone and several convolution layers; ‘+MSA’: Baseline with MSA; ‘w/TA only’: Baseline equipped with TA and iterative refinement fashion.

Settings	Decoder			NC4K (4,121)				COD10K-Test (2,026)				CAMO-Test (250)			
	TA	F-TA	B-TA	$S_m \uparrow$	$\alpha E \uparrow$	$wF \uparrow$	$M \downarrow$	$S_m \uparrow$	$\alpha E \uparrow$	$wF \uparrow$	$M \downarrow$	$S_m \uparrow$	$\alpha E \uparrow$	$wF \uparrow$	$M \downarrow$
1				0.865	0.921	0.795	0.041	0.836	0.915	0.724	0.030	0.857	0.915	0.797	0.053
2	✓			0.880	0.925	0.825	0.034	0.850	0.908	0.749	0.026	0.862	0.918	0.812	0.055
3		✓		0.878	0.924	0.812	0.036	0.849	0.909	0.742	0.028	0.861	0.916	0.811	0.054
4			✓	0.875	0.920	0.815	0.038	0.845	0.915	0.742	0.029	0.856	0.914	0.809	0.055
5		✓	✓	0.880	0.928	0.827	0.035	0.847	0.919	0.754	0.024	0.862	0.921	0.812	0.052
6	✓		✓	0.885	0.933	0.839	0.033	0.860	0.924	0.763	0.025	0.866	0.926	0.827	0.048
7	✓	✓		0.889	0.939	0.845	0.031	0.866	0.927	0.773	0.024	0.871	0.929	0.832	0.046
8	✓	✓	✓	0.892	0.941	0.847	0.030	0.869	0.931	0.786	0.023	0.872	0.931	0.831	0.046

Table 4. Ablation study on the proposed MSA. All three branches (‘TA’, ‘F-TA’, and ‘B-TA’) contribute to the overall performance. In addition, eliminating either the ‘F-TA’ or ‘B-TA’ branch hurts the performance.

DTINet [35], UGTR [60], and ICON [71]. For a fair comparison, the prediction results are directly provided by their authors or generated by their well-trained models.

Performance on Object Regions. As shown in Tab. 1, our proposed CamoFormer consistently and significantly surpasses the previous methods on all three benchmarks without any post-process tricks or extra data for training. Compared to the recent CNN-based COD methods, such as ZoomNet [41], FDNet [70], and SegMaR [22], although they adopt strategies, like multi-stage training and inference that cost extra computational burden, our CamoFormer still outperforms them on all benchmarks by a large margin. Meanwhile, compared to the Transformer-based models (*e.g.*, TPRNet [67] and DTINet [35]), our method also performs better than them, setting new SOTA records.

Performance on Border Regions. The borders of camouflaged targets are challenging to detect due to their irregular shapes and high similarity with their surroundings. In order to quantify the segmentation performance near the border regions, we calculate the wF and MAE scores in the border regions, denoted as BR- wF and BR-M, respectively. We attain the border regions by dilating the boundaries of the GT objects, as shown in Fig. 6. Note that the area of the region depends on the kernel size of the dilation operation. Tab. 2 shows the performance calculated in the border regions ‘BR@15’ and ‘BR@30’. Remarkably, CamoFormer achieves much better results than other methods, demonstrating that our predictions perform better at GT object boundaries, while the predictions of other methods are significantly biased.

4.4. Model Sweep

Overall Results. We first ablate the network architecture of CamoFormer. The results are shown in Tab. 3. The ‘Baseline’ refers to the model with only the encoder followed by a convolution for prediction. When our MSA is applied, the performance can be clearly improved in terms of all evaluation metrics compared to the ‘Baseline’. Then, we attempt to add the decoder with only TA left. This progressive fusion strategy also helps compared to the ‘Baseline’. Finally, we add our MSA in the decoder as in Fig. 2. We can see that the performance can be further improved. Both the top and bottom halves indicate the importance of MSA for COD.

Masked Separable Attention. We then ablate how each component in MSA helps. Tab. 4 shows the experimental results. The ‘Baseline’ in the first row can be viewed as a simple feature pyramid network, *i.e.*, no MSA is added in Fig. 2. We can observe that each type of attention component is helpful to improve performance. Though TA yields more performance gain compared to F-TA and B-TA, combining either F-TA or B-TA with TA can further improve the results. In particular, adding all three components yields the best results on all three datasets. This series of experiments indicate that separately processing the foreground and background with the proposed MSA is useful for segmenting the camouflaged objects.

Feature Visualization. To provide more promising insights into our MSA, we also visualize the features around it. Note that the MSA of Stages 2 and 5 are chosen for visualization. As shown in Fig. 7, F-TA and B-TA are able to effectively

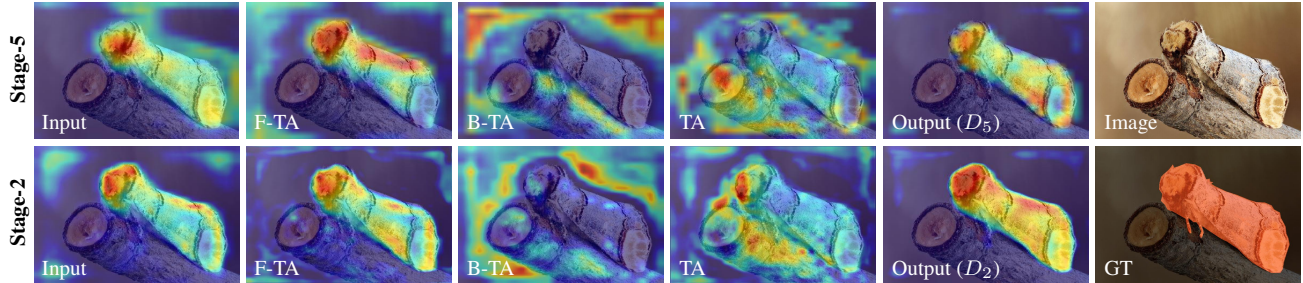


Figure 7. Visualization of the feature maps around MSA. The features from Stage 2 and Stage 5 are chosen for comparison.

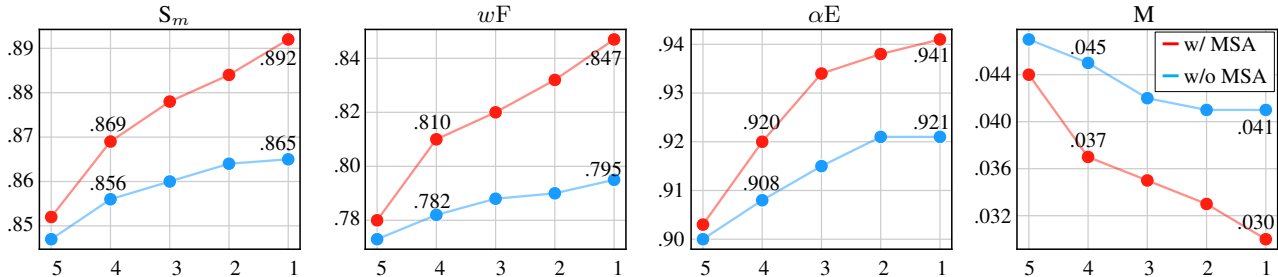


Figure 8. Performance on the NC4K dataset at different feature levels of our progressive fusion strategy. The proposed MSA fits well with the decoder in that the performance gap tends to be larger from feature level 5 to feature level 1.

obtain the cues of the foreground and background. The features from F-TA, B-TA, and TA are complementary to form a completely camouflaged object. Consequently, the precise location and detailed information of the camouflaged object can be captured easily. In addition, compared to the features in Stage 5, we can distinguish the camouflaged targets more clearly according to the ones in Stage 2, which indicates that the progressive refinement decoder can fully exploit the potential of our MSA.

MSA in Progressive Fusion. In our model, a progressive fusion strategy is adopted to gradually refine the segmentation map in the decoder. To show the impact of our MSA in this strategy, we depict the performance curves at different feature levels under the setup of w/ MSA and w/o MSA. The results can be found in Fig. 8. We can see that from feature level 5 to feature level 1, the performance gap between the model without MSA (blue line) and the one with MSA tends to be more significant for all four evaluation metrics. This indicates that the proposed MSA is compatible with the progressive fusion decoder.

Decoder Width. The width (#channels) of the decoder affects not only the model size but also the inference speed. Tab. 5 shows the changes in model parameters, computational cost, and performance when the number of channels changes. We can see a clear improvement in our model when C_d increases from 32 to 128. However, when the width changes from 128 to 192, the performance improves little, but the parameters and computations rise. As a re-

Settings	Computations		NC4K		COD10K-Test	
	Params	MAC	$S_m \uparrow$	$wF \uparrow$	$S_m \uparrow$	$wF \uparrow$
$C_d = 32$	63M	30G	0.887	0.842	0.865	0.779
$C_d = 64$	65M	34G	0.890	0.846	0.869	0.784
$C_d = 128$	71M	47G	0.892	0.847	0.869	0.786
$C_d = 192$	82M	69G	0.892	0.849	0.868	0.786
$C_d = 256$	97M	99G	0.891	0.846	0.866	0.784

Table 5. Ablation study on the channel numbers in the decoder. All the variants are equipped with our MSA. More comparisons are shown in the supplementary materials.

sult, C_d is set to 128 for the trade-off between efficiency and model performance. This is different from most previous FPN-based methods [18, 30] that use larger channel numbers at deeper feature levels.

5. Conclusions

We present CamoFormer for camouflaged object segmentation. The core of our CamoFormer is the masked separable attention (MSA) that separately deals with the foreground and background regions using different attention heads. To make better use of our MSA, we adopt a progressive refinement decoder to gradually improve the segmentation quality at different feature levels in a top-down manner. Extensive experiments show that CamoFormer surpasses the existing 18 SOTA models with clear improvements. We hope our MSA can facilitate the development of COD and other binary segmentation tasks.

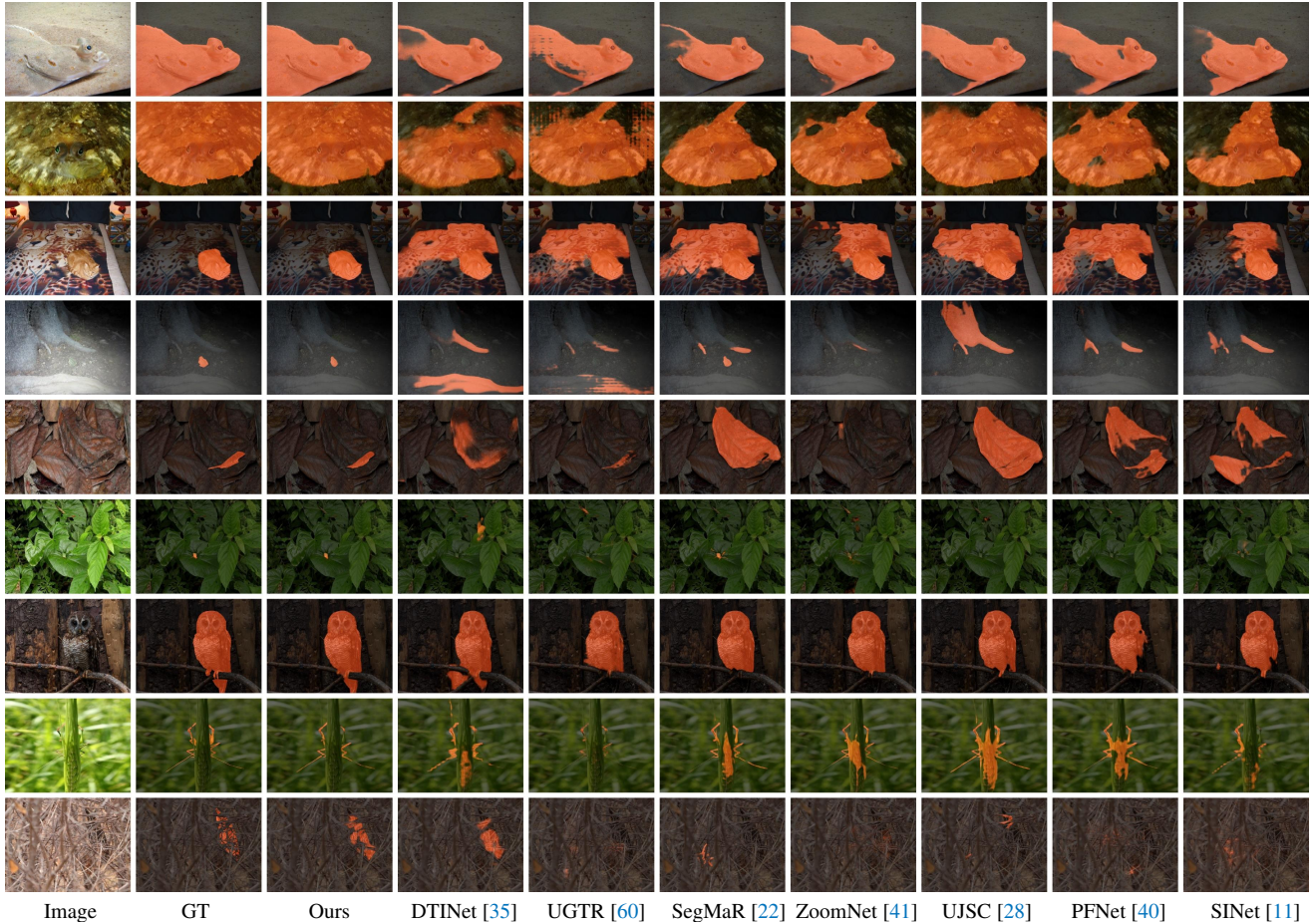


Figure 9. More visual example comparisons between our CamoFormer and some previous SOTA methods. Segmentation results are highlighted in orange.

Settings	Computations		NC4K				COD10K-Test				CAMO			
	Params	MAC	$S_m \uparrow$	αE	$wF \uparrow$	M	$S_m \uparrow$	αE	$wF \uparrow$	M	$S_m \uparrow$	αE	$wF \uparrow$	M
$C_d = 32$	63M	30G	0.887	0.938	0.842	0.031	0.865	0.925	0.779	0.024	0.871	0.926	0.827	0.047
$C_d = 64$	65M	34G	0.890	0.940	0.846	0.031	0.869	0.929	0.784	0.023	0.872	0.931	0.829	0.047
$C_d = 128$	71M	47G	0.892	0.941	0.847	0.030	0.869	0.931	0.786	0.023	0.872	0.931	0.831	0.046
$C_d = 192$	82M	69G	0.892	0.942	0.849	0.030	0.868	0.932	0.786	0.023	0.873	0.933	0.834	0.046
$C_d = 256$	97M	99G	0.891	0.942	0.846	0.030	0.866	0.932	0.784	0.023	0.869	0.931	0.830	0.046

Table 6. Detailed ablation study on the channel numbers in the decoder of our CamoFormer.

Acknowledgements

Qibin Hou was partially supported by the Natural Science Foundation of China (No. 62276145) and the Fundamental Research Funds for the Central Universities (No. 63223049).

A. Performance on All Benchmark Datasets

In the main paper, we have provided the evaluation results of our CamoFormer on the three most popular benchmark datasets, namely NC4K, COD10K-Test,

and CAMO-Test. Here, we also report the results on CHAMELEON [46], which contains 76 image-annotation pairs. As shown in Tab. 7, our CamoFormer can improve all other methods significantly.

B. More Visual Comparisons

We show more visualization examples of our CamoFormer and the recent SOTA methods in Fig. 9. These examples cover a wide range of camouflaged scenes, such as big objects, small objects, occlusion, and indefinable

Method	NC4K (4,121)				COD10K-Test (2,026)				CAMO-Test (250)				CHAMELEON (76)			
	$S_m \uparrow$	$\alpha E \uparrow$	$wF \uparrow$	$M \downarrow$	$S_m \uparrow$	$\alpha E \uparrow$	$wF \uparrow$	$M \downarrow$	$S_m \uparrow$	$\alpha E \uparrow$	$wF \uparrow$	$M \downarrow$	$S_m \uparrow$	$\alpha E \uparrow$	$wF \uparrow$	$M \downarrow$
<i>CNN-Based Methods</i>																
PraNet ₂₀₂₀ [12]	.822	.871	.724	.059	.789	.839	.629	.045	.769	.833	.663	.094	.860	.898	.763	.044
SINet ₂₀₂₀ [11]	.808	.883	.723	.058	.776	.867	.631	.043	.745	.825	.644	.092	.872	.938	.806	.034
SLSR ₂₀₂₁ [36]	.840	.902	.766	.048	.804	.882	.673	.037	.787	.855	.696	.080	.890	.936	.822	.030
MGL-R ₂₀₂₁ [64]	.833	.893	.739	.053	.814	.865	.666	.035	.782	.847	.695	.085	.893	.923	.812	.031
PFNet ₂₀₂₁ [40]	.829	.892	.745	.053	.800	.868	.660	.040	.782	.852	.695	.085	.882	.942	.810	.033
UJSC ₂₀₂₁ [28]	.842	.907	.771	.047	.809	.891	.684	.035	.800	.853	.728	.073	.891	.943	.833	.030
C²FNet ₂₀₂₁ [49]	.838	.898	.762	.049	.813	.886	.686	.036	.796	.864	.719	.080	.888	.932	.828	.032
SINetV2 ₂₀₂₂ [10]	.847	.898	.770	.048	.815	.863	.680	.037	.820	.875	.743	.070	.888	.930	.816	.030
DGNet ₂₀₂₂ [20]	.857	.907	.784	.042	.822	.877	.693	.033	.839	.901	.769	.057	.890	.934	.816	.029
SegMaR ₂₀₂₂ [22]	.841	.905	.781	.046	.833	.895	.724	.033	.815	.872	.742	.071	.897	.950	.835	.027
ZoomNet ₂₀₂₂ [41]	.853	.907	.784	.043	.838	.893	.729	.029	.820	.883	.752	.066	.902	.952	.845	.023
FDNet ₂₀₂₂ [70]	.834	.895	.750	.052	.837	.897	.731	.030	.844	.903	.778	.062	.894	.948	.819	.030
CamoFormer-R (Ours)	.857	.915	.793	.041	.838	.898	.730	.029	.817	.884	.756	.066	.900	.949	.843	.024
CamoFormer-C (Ours)	.884	.936	.833	.033	.860	.923	.767	.024	.860	.920	.811	.051	.901	.955	.846	.025
<i>Transformer-Based Methods</i>																
COS-T ₂₀₂₁ [53]	.825	.881	.730	.055	.790	.901	.693	.035	.813	.896	.776	.060	.885	.948	.854	.025
VST ₂₀₂₁ [32]	.830	.887	.740	.053	.810	.866	.680	.035	.805	.863	.780	.069	.888	.936	.820	.033
UGTR ₂₀₂₁ [60]	.839	.886	.746	.052	.817	.850	.666	.036	.784	.859	.794	.086	.888	.921	.794	.031
ICON ₂₀₂₂ [71]	.858	.914	.782	.041	.818	.882	.688	.033	.840	.902	.769	.058	.854	.920	.763	.037
TPRNet ₂₀₂₂ [67]	.854	.903	.790	.047	.829	.892	.725	.034	.814	.870	.781	.076	.891	.930	.816	.031
DTINet ₂₀₂₂ [35]	.863	.915	.792	.041	.824	.893	.695	.034	.857	.912	.796	.050	.883	.928	.813	.033
CamoFormer-S (Ours)	.888	.941	.840	.031	.862	.932	.772	.024	.876	.935	.832	.043	.891	.953	.829	.026
CamoFormer-P (Ours)	.892	.941	.847	.030	.869	.931	.786	.023	.872	.931	.831	.046	.910	.970	.865	.022

Table 7. Comparison of our CamoFormer with the recent SOTA methods on four datasets. ‘-R’: ResNet [17], ‘-C’: ConvNext [34], ‘-S’: Swin Transformer [33], ‘-P’: PVTv2 [55], ‘ \uparrow ’: the higher the better, ‘ \downarrow ’: the lower the better.

boundaries. Obviously, our CamoFormer performs much better than other methods.

C. More Ablation Results of Decoder Channels

The ablation results of the decoder channels on three benchmark datasets are shown in Tab. 6. We adopt $C_d = 128$ for the trade-off between performance and computations. It is noteworthy that our CamoFormer can outperform other previous methods even if $C_d = 32$ is applied.

D. PR & F_β curves of COD methods

We provide the PR and F_β curves of our CamoFormer and previous methods on NC4K, CAMO, and COD10K datasets, as shown in Fig. 10. Note that the higher the curve is, the better the model performs. It is clear that our CamoFormer (red curve) surpasses all other methods.

References

[1] Yevgeny Beiderman, Mina Teicher, Javier Garcia, Vicente Mico, and Zeev Zalevsky. Optical technique for classification, recognition and identification of obscured objects. *Opt. Commun.*, 283(21):4274–4282, 2010. 2

[2] Nicolas Carion, Francisco Massa, Gabriel Synnaeve, Nicolas Usunier, Alexander Kirillov, and Sergey Zagoruyko. End-to-end object detection with transformers. In *ECCV*, 2020. 2

[3] Bowen Cheng, Ishan Misra, Alexander G Schwing, Alexander Kirillov, and Rohit Girdhar. Masked-attention mask transformer for universal image segmentation. In *IEEE CVPR*, 2022. 1

[4] Xiangxiang Chu, Zhi Tian, Yuqing Wang, Bo Zhang, Haibing Ren, Xiaolin Wei, Huaxia Xia, and Chunhua Shen. Twins: Revisiting the design of spatial attention in vision transformers. In *NeurIPS*, 2021. 2

[5] Pieter-Tjerk De Boer, Dirk P Kroese, Shie Mannor, and Reuven Y Rubinfeld. A tutorial on the cross-entropy method. *Ann. Oper. Res.*, 134(1):19–67, 2005. 4

[6] Jacob Devlin, Ming-Wei Chang, Kenton Lee, and Kristina Toutanova. Bert: Pre-training of deep bidirectional transformers for language understanding. In *NAACL*, 2018. 2

[7] Alexey Dosovitskiy, Lucas Beyer, Alexander Kolesnikov, Dirk Weissenborn, Xiaohua Zhai, Thomas Unterthiner, Mostafa Dehghani, Matthias Minderer, Georg Heigold, Sylvain Gelly, et al. An image is worth 16x16 words: Transformers for image recognition at scale. In *ICLR*, 2020. 2

[8] Deng-Ping Fan, Ming-Ming Cheng, Yun Liu, Tao Li, and Ali Borji. Structure-measure: A new way to evaluate foreground maps. In *IEEE ICCV*, 2017. 5

[9] Deng-Ping Fan, Cheng Gong, Yang Cao, Bo Ren, Ming-Ming Cheng, and Ali Borji. Enhanced-alignment measure

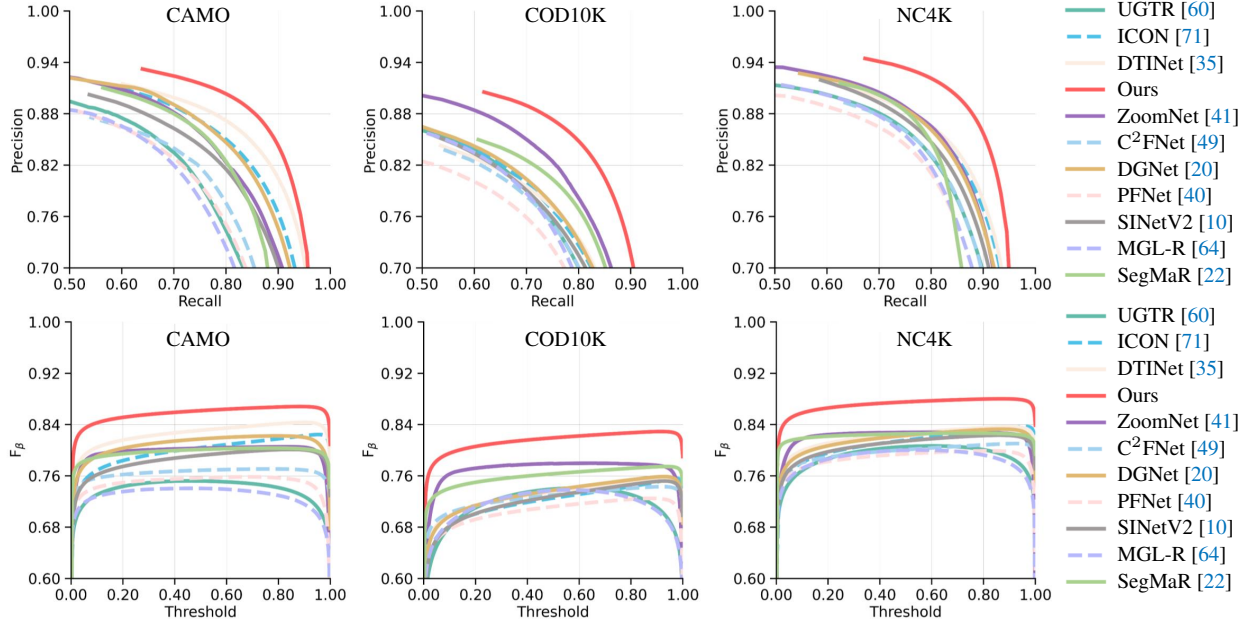


Figure 10. PR and f_β curves of the proposed CamoFormer and the recent SOTA algorithms on three COD datasets.

- for binary foreground map evaluation. In *IJCAI*, 2018. 5
- [10] Deng-Ping Fan, Ge-Peng Ji, Ming-Ming Cheng, and Ling Shao. Concealed object detection. *IEEE TPAMI*, 44(10):6024–6042, 2022. 1, 2, 4, 5, 6, 10, 11
- [11] Deng-Ping Fan, Ge-Peng Ji, Guolei Sun, Ming-Ming Cheng, Jianbing Shen, and Ling Shao. Camouflaged object detection. In *IEEE CVPR*, 2020. 1, 2, 3, 5, 6, 9, 10
- [12] Deng-Ping Fan, Ge-Peng Ji, Tao Zhou, Geng Chen, Huazhu Fu, Jianbing Shen, and Ling Shao. Pranet: Parallel reverse attention network for polyp segmentation. In *MICCAI*, 2020. 1, 3, 6, 10
- [13] Meirav Galun, Eitan Sharon, Ronen Basri, and Achi Brandt. Texture segmentation by multiscale aggregation of filter responses and shape elements. In *IEEE ICCV*, 2003. 2
- [14] Hongxing Guo, Yaling Dou, Ting Tian, Jingli Zhou, and Shengsheng Yu. A robust foreground segmentation method by temporal averaging multiple video frames. In *IEEE ICALIP*, 2008. 2
- [15] Joanna R Hall, Innes C Cuthill, Roland Baddeley, Adam J Shohet, and Nicholas E Scott-Samuel. Camouflage, detection and identification of moving targets. *Proc. Royal Soc. B*, 280(1758):20130064, 2013. 2
- [16] Kai Han, An Xiao, Enhua Wu, Jianyuan Guo, Chunjing Xu, and Yunhe Wang. Transformer in transformer. In *NeurIPS*, 2021. 2
- [17] Kaiming He, Xiangyu Zhang, Shaoqing Ren, and Jian Sun. Deep residual learning for image recognition. In *IEEE CVPR*, 2016. 2, 5, 6, 10
- [18] Qibin Hou, Ming-Ming Cheng, Xiaowei Hu, Ali Borji, Zhuowen Tu, and Philip Torr. Deeply supervised salient object detection with short connections. *IEEE TPAMI*, 41(4):815–828, 2019. 4, 8
- [19] Jie Hu, Li Shen, and Gang Sun. Squeeze-and-excitation networks. In *IEEE CVPR*, 2018. 2
- [20] Ge-Peng Ji, Deng-Ping Fan, Yu-Cheng Chou, Dengxin Dai, Alexander Liniger, and Luc Van Gool. Deep gradient learning for efficient camouflaged object detection. *MIR*, 2022. doi: <https://doi.org/10.1007/s11633-022-1365-9>. 1, 6, 10, 11
- [21] Ge-Peng Ji, Lei Zhu, Mingchen Zhuge, and Keren Fu. Fast camouflaged object detection via edge-based reversible recalibration network. *PR*, 123:108414, 2022. 2
- [22] Qi Jia, Shuilian Yao, Yu Liu, Xin Fan, Risheng Liu, and Zhongxuan Luo. Segment, magnify and reiterate: Detecting camouflaged objects the hard way. In *IEEE CVPR*, 2022. 1, 2, 3, 5, 6, 7, 9, 10, 11
- [23] Xinhao Jiang, Wei Cai, Zhili Zhang, Bo Jiang, Zhiyong Yang, and Xin Wang. Magnet: A camouflaged object detection network simulating the observation effect of a magnifier. *arXiv*, 2022. doi: <https://doi.org/10.21203/rs.3.rs-1020529/v2>. 3
- [24] Zi-Hang Jiang, Qibin Hou, Li Yuan, Daquan Zhou, Yujun Shi, Xiaojie Jin, Anran Wang, and Jiashi Feng. All tokens matter: Token labeling for training better vision transformers. In *NeurIPS*, 2021. 2
- [25] Ch Kavitha, B Prabhakara Rao, and A Govardhan. An efficient content based image retrieval using color and texture of image sub blocks. *IJEST*, 3(2):1060–1068, 2011. 2
- [26] Alex Krizhevsky, Ilya Sutskever, and Geoffrey E Hinton. Imagenet classification with deep convolutional neural networks. *Commun. ACM*, 60(6):84–90, 2017. 5
- [27] Trung-Nghia Le, Tam V Nguyen, Zhongliang Nie, Minh-Triet Tran, and Akihiro Sugimoto. Anabranh network for camouflaged object segmentation. *CVIU*, 184:45–56, 2019. 2, 4, 5

- [28] Aixuan Li, Jing Zhang, Yunqiu Lv, Bowen Liu, Tong Zhang, and Yuchao Dai. Uncertainty-aware joint salient object and camouflaged object detection. In *IEEE CVPR*, 2021. 2, 6, 9, 10
- [29] Tsung-Yi Lin, Piotr Dollár, Ross Girshick, Kaiming He, Bharath Hariharan, and Serge Belongie. Feature pyramid networks for object detection. In *IEEE CVPR*, 2017. 2
- [30] Jiang-Jiang Liu, Qibin Hou, Ming-Ming Cheng, Jiashi Feng, and Jianmin Jiang. A simple pooling-based design for real-time salient object detection. In *IEEE CVPR*, 2019. 2, 8
- [31] Li Liu, Wanli Ouyang, Xiaogang Wang, Paul Fieguth, Jie Chen, Xinwang Liu, and Matti Pietikäinen. Deep learning for generic object detection: A survey. *IJCV*, 128(2):261–318, 2020. 1
- [32] Nian Liu, Ni Zhang, Kaiyuan Wan, Ling Shao, and Junwei Han. Visual saliency transformer. In *IEEE ICCV*, 2021. 2, 3, 6, 10
- [33] Ze Liu, Yutong Lin, Yue Cao, Han Hu, Yixuan Wei, Zheng Zhang, Stephen Lin, and Baining Guo. Swin transformer: Hierarchical vision transformer using shifted windows. In *IEEE ICCV*, 2021. 5, 6, 10
- [34] Zhuang Liu, Hanzhi Mao, Chao-Yuan Wu, Christoph Feichtenhofer, Trevor Darrell, and Saining Xie. A convnet for the 2020s. In *IEEE CVPR*, 2022. 5, 6, 10
- [35] Zhengyi Liu, Zhili Zhang, and Wei Wu. Boosting camouflaged object detection with dual-task interactive transformer. *ICPR*, 2022. 2, 6, 7, 9, 10, 11
- [36] Yunqiu Lv, Jing Zhang, Yuchao Dai, Aixuan Li, Bowen Liu, Nick Barnes, and Deng-Ping Fan. Simultaneously localize, segment and rank the camouflaged objects. In *IEEE CVPR*, 2021. 2, 4, 5, 6, 10
- [37] Ran Margolin, Lihi Zelnik-Manor, and Ayellet Tal. How to evaluate foreground maps? In *IEEE CVPR*, 2014. 5
- [38] Gellért Mátyus, Wenjie Luo, and Raquel Urtasun. Deep-roadmapper: Extracting road topology from aerial images. In *IEEE ICCV*, 2017. 4
- [39] Gerard Medioni. Generic object recognition by inference of 3-d volumetric. *Object Categorization: Computer and Human Vision Perspectives*, 87, 2009. 1
- [40] Haiyang Mei, Ge-Peng Ji, Ziqi Wei, Xin Yang, Xiaopeng Wei, and Deng-Ping Fan. Camouflaged object segmentation with distraction mining. In *IEEE CVPR*, 2021. 1, 2, 6, 9, 10, 11
- [41] Youwei Pang, Xiaoqi Zhao, Tian-Zhu Xiang, Lihe Zhang, and Huchuan Lu. Zoom in and out: A mixed-scale triplet network for camouflaged object detection. In *IEEE CVPR*, 2022. 1, 2, 3, 5, 6, 7, 9, 10, 11
- [42] Adam Paszke, Sam Gross, Francisco Massa, Adam Lerer, James Bradbury, Gregory Chanan, Trevor Killeen, Zeming Lin, Natalia Gimelshein, Luca Antiga, et al. Pytorch: An imperative style, high-performance deep learning library. In *NeurIPS*, 2019. 5
- [43] Federico Perazzi, Philipp Krähenbühl, Yael Pritch, and Alexander Hornung. Saliency filters: Contrast based filtering for salient region detection. In *IEEE CVPR*, 2012. 5
- [44] Ilija Radosavovic, Raj Prateek Kosaraju, Ross Girshick, Kaiming He, and Piotr Dollár. Designing network design spaces. In *IEEE CVPR*, 2020. 2
- [45] Karen Simonyan and Andrew Zisserman. Very deep convolutional networks for large-scale image recognition. *ICLR*, 2015. 2
- [46] Przemysław Skurowski, Hassan Abdulameer, J Błaszczczyk, Tomasz Depta, Adam Kornacki, and P Kozieł. Animal camouflage analysis: Chameleon database. *Unpublished manuscript*, 2018. 9
- [47] Aravind Srinivas, Tsung-Yi Lin, Niki Parmar, Jonathon Shlens, Pieter Abbeel, and Ashish Vaswani. Bottleneck transformers for visual recognition. In *IEEE CVPR*, 2021. 2
- [48] Martin Stevens and Sami Merilaita. Animal camouflage: current issues and new perspectives. *Philos. Trans. R. Soc. Lond., B, Biol. Sci.*, 364(1516):423–427, 2009. 1
- [49] Yujia Sun, Geng Chen, Tao Zhou, Yi Zhang, and Nian Liu. Context-aware cross-level fusion network for camouflaged object detection. In *IJCAI*, 2021. 6, 10, 11
- [50] Christian Szegedy, Vincent Vanhoucke, Sergey Ioffe, Jon Shlens, and Zbigniew Wojna. Rethinking the inception architecture for computer vision. In *IEEE CVPR*, 2016. 2
- [51] Hugo Touvron, Matthieu Cord, Matthijs Douze, Francisco Massa, Alexandre Sablayrolles, and Hervé Jégou. Training data-efficient image transformers & distillation through attention. In *ICML*, 2021. 2
- [52] Ashish Vaswani, Noam Shazeer, Niki Parmar, Jakob Uszkoreit, Llion Jones, Aidan N Gomez, Łukasz Kaiser, and Illia Polosukhin. Attention is all you need. In *NeurIPS*, 2017. 2, 4
- [53] Haiwen Wang, Xinzhou Wang, Fuchun Sun, and Yixu Song. Camouflaged object segmentation with transformer. In *ICCSIP*, 2021. 6, 10
- [54] Wenhai Wang, Enze Xie, Xiang Li, Deng-Ping Fan, Kaitao Song, Ding Liang, Tong Lu, Ping Luo, and Ling Shao. Pyramid vision transformer: A versatile backbone for dense prediction without convolutions. In *IEEE ICCV*, 2021. 2
- [55] Wenhai Wang, Enze Xie, Xiang Li, Deng-Ping Fan, Kaitao Song, Ding Liang, Tong Lu, Ping Luo, and Ling Shao. Pvt v2: Improved baselines with pyramid vision transformer. *CVMJ*, 8(3):415–424, 2022. 3, 5, 6, 10
- [56] Haiping Wu, Bin Xiao, Noel Codella, Mengchen Liu, Xiyang Dai, Lu Yuan, and Lei Zhang. Cvt: Introducing convolutions to vision transformers. In *IEEE ICCV*, 2021. 2
- [57] Enze Xie, Wenhai Wang, Zhiding Yu, Anima Anandkumar, Jose M Alvarez, and Ping Luo. Segformer: Simple and efficient design for semantic segmentation with transformers. In *NeurIPS*, 2021. 2
- [58] Saining Xie and Zhuowen Tu. Holistically-nested edge detection. In *IEEE ICCV*, 2015. 4
- [59] Weijian Xu, Yifan Xu, Tyler Chang, and Zhuowen Tu. Co-scale conv-attentional image transformers. In *IEEE ICCV*, 2021. 2
- [60] Fan Yang, Qiang Zhai, Xin Li, Rui Huang, Ao Luo, Hong Cheng, and Deng-Ping Fan. Uncertainty-guided transformer reasoning for camouflaged object detection. In *IEEE ICCV*, 2021. 2, 6, 7, 9, 10, 11
- [61] Jianwei Yang, Chunyuan Li, Pengchuan Zhang, Xiyang Dai, Bin Xiao, Lu Yuan, and Jianfeng Gao. Focal attention for

- long-range interactions in vision transformers. In *NeurIPS*, 2021. 2
- [62] Li Yuan, Qibin Hou, Zihang Jiang, Jiashi Feng, and Shuicheng Yan. Volo: Vision outlooker for visual recognition. *IEEE TPAMI*, 2022. doi:<https://doi.org/10.1109/TPAMI.2022.3206108>. 2
- [63] Syed Waqas Zamir, Aditya Arora, Salman Khan, Munawar Hayat, Fahad Shahbaz Khan, and Ming-Hsuan Yang. Restormer: Efficient transformer for high-resolution image restoration. In *IEEE CVPR*, 2022. 1, 4
- [64] Qiang Zhai, Xin Li, Fan Yang, Chenglizhao Chen, Hong Cheng, and Deng-Ping Fan. Mutual graph learning for camouflaged object detection. In *IEEE CVPR*, 2021. 6, 10, 11
- [65] Jing Zhang, Jianwen Xie, Nick Barnes, and Ping Li. Learning generative vision transformer with energy-based latent space for saliency prediction. In *NeurIPS*, 2021. 3
- [66] Miao Zhang, Shuang Xu, Yongri Piao, Dongxiang Shi, Shusen Lin, and Huchuan Lu. Preynet: Preying on camouflaged objects. In *ACM MM*, 2022. 2
- [67] Qiao Zhang, Yanliang Ge, Cong Zhang, and Hongbo Bi. Tprnet: camouflaged object detection via transformer-induced progressive refinement network. *TVCI*, pages 1–15, 2022. 2, 6, 7, 10
- [68] Xiang Zhang, Ce Zhu, Shuai Wang, Yipeng Liu, and Mao Ye. A bayesian approach to camouflaged moving object detection. *IEEE TCSVT*, 27(9):2001–2013, 2016. 2
- [69] Sixiao Zheng, Jiachen Lu, Hengshuang Zhao, Xiatian Zhu, Zekun Luo, Yabiao Wang, Yanwei Fu, Jianfeng Feng, Tao Xiang, Philip HS Torr, et al. Rethinking semantic segmentation from a sequence-to-sequence perspective with transformers. In *IEEE CVPR*, 2021. 2
- [70] Yijie Zhong, Bo Li, Lv Tang, Senyun Kuang, Shuang Wu, and Shouhong Ding. Detecting camouflaged object in frequency domain. In *IEEE CVPR*, 2022. 1, 2, 3, 5, 6, 7, 10
- [71] Mingchen Zhuge, Deng-Ping Fan, Nian Liu, Dingwen Zhang, Dong Xu, and Ling Shao. Salient object detection via integrity learning. *IEEE TPAMI*, 2022. doi:<https://doi.org/10.1109/TPAMI.2022.3179526>. 2, 6, 7, 10, 11
- [72] Mingchen Zhuge, Xiankai Lu, Yiyu Guo, Zhihua Cai, and Shuhan Chen. Cubenet: X-shape connection for camouflaged object detection. *PR*, 127:108644, 2022. 2